longitudinal and transverse relaxation time constants T_1 and T_2 were measured using standard inversion–recovery and Carr–Purcell–Meiboom–Gill pulse sequences[23], giving $T_1 \approx 19$ and 25 s, and $T_2 \approx 7$ and 0.3 s, respectively, for proton and carbon; these were much longer than required for our experiment, which finished in about 7 ms.

The single most important source of errors in the experiments was the radiofrequency field inhomogeneity and pulse-length calibration imperfections. A direct measure of this inhomogeneity is the ~200-μs time constant of the exponentially decaying envelope observed from applying a single pulse as a function of pulse length. Including the population permutation sequence, about 7 pulses are applied to each nucleus, with a cumulative duration of ~70–100 μs.

The second most important contribution to errors is the low carbon signal-to-noise ratio, signal peak height/r.m.s. noise ≈35, versus about 4,300 for proton. The carbon signal was much weaker because the carbon gyromagnetic ratio is 4 times smaller, and the carbon receiver coil is mounted more remotely from the sample. Smaller contributions to errors came from incomplete relaxation between subsequent experiments, carrier frequency offsets and numerical errors in the data analysis.

For this small-scale quantum computer, imperfections were dominated by technology, rather than by fundamental issues. However, NMR quantum computers larger than about 10 qubits will require creative new approaches, because the signal strength decays exponentially with the number of qubits in the machine, using current schemes[24,25]: for N spins, the signal from the initial state 00…0 is proportional to $n_{00\ldots0} \propto NZ^{-N}$, where the single spin partition function $Z \approx 2$ at high temperatures. Furthermore, coherence times typically decrease for larger molecules, whereas the average logic gate duration increases. Nevertheless, there is hope; for example, because of the ensemble nature of the NMR approach, the output result can be inferred as long as a distinguishable majority of the molecules reach the correct final state. Creating an effective pure state is thus not always necessary, as we have demonstrated. Optical pumping and other cooling techniques can also be used to prepolarize the sample to increase the output signal amplitude, because $Z \approx 1$ at low temperatures. Quantum computation poses an interesting and relevant experimental challenge for the future.

Note added in proof: During the course of this work, we became aware of a closely related experiment by J. A. Jones and M. Mosca[26].

Received 21 January; accepted 18 March 1998.

1. Deutsch, D. Quantum theory, the Church-Turing principle and the universal quantum computer. *Proc. R. Soc. Lond. A* **400,** 97–117 (1985).
2. Shor, P. Algorithms for quantum computation: discrete logarithms and factoring. *Proc. 35th Annu. Symp. on Found. of Computer Science* 124–134 (IEEE Comp. Soc. Press, Los Alomitos, CA, 1994).
3. Divincenzo, D. P. Quantum computation. *Science* **270,** 255–261 (1995).
4. Lloyd, S. Quantum-mechanical computers. *Sci. Am.* **273,** 44–50 (1995).
5. Ekert, A. & Jozsa, R. Quantum computation and Shor's factoring algorithm. *Rev. Mod. Phys.* **68,** 733–753 (1996).
6. Deutsch, D. & Jozsa, R. Rapid solution of problems by quantum computation. *Proc. R. Soc. Lond. A* **439,** 553–558 (1992).
7. Simon, D. On the power of quantum computation. *Proc. 35th Annu. Symp. on Found. of Computer Science* 116–124 (IEEE Comp. Soc. Press, Los Alamitos, CA, 1994).
8. Grover, L. K. Quantum computers can search arbitrarily large databases by a single query. *Phys. Rev. Lett.* **79,** 4709–4012 (1997).
9. Unruh, W. G. Maintaining coherence in quantum computers. *Phys. Rev. A* **51,** 2, 992–997 (1995).
10. Chuang, I. L., Laflamme, R., Shor, P. & Zurek, W. H. Quantum computers, factoring, and decoherence. *Science* **270,** 1633–1635 (1995).
11. Landauer, R. Dissipation and noise immunity in computation and communication. *Nature* **335,** 779–784 (1988).
12. Landauer, R. Is quantum mechanics useful? *Phil. Trans. R. Soc. Lond. A* **335,** 367–376 (1995).
13. Palma, G. M., Suominen, K.-A. & Ekert, A. K. Quantum computers and dissipation. *Proc. R. Soc. Lond A* **452,** 567–584 (1996).
14. Monroe, C., Meekhof, D. M., King, B. E., Itano, W. M. & Wineland, D. J. Demonstration of a fundamental quantum logic gate. *Phys. Rev. Lett.* **75,** 4714–4717 (1995).
15. Turchette, Q. A., Hood, C. J., Lange, W., Mabuchi, H. & Kimble, H. J. Measurement of conditional phase shifts for quantum logic. *Phys. Rev. Lett.* **75,** 4710–4713 (1995).
16. Gershenfeld, N. & Chuang, I. L. Bulk spin-resonance quantum computation. *Science* **275,** 350–356 (1997).
17. Cory, D. G., Price, M. D., Fahmy, A. F. & Havel, T. F. Nuclear magnetic resonance spectroscopy: an experimentally accessible paradigm for quantum computing. *Physica D* (in the press; LANL E-print quant-ph/9709001.gov, 1997).
18. Cory, D. G., Fahmy, A. F. & Havel, T. F. Ensemble quantum computing by NMR spectroscopy. *Proc. Natl Acad. Sci. USA* **94,** 1634–1639 (1997).
19. Lloyd, S. A potentially realizable quantum computer. *Science* **261,** 1569–1571 (1993).
20. Cleve, R., Ekert, A., Macchiavello, C. & Mosca, M. *Proc. R. Soc. Lond. A* **454,** 339–354 (1998). LANL E-prin quant-ph/9708016.
21. Slichter, C. P. *Principles of Magnetic Resonance* (Springer, Berlin, 1990).
22. Knill, E., Chuang, I. L. & Laflamme, R. Effective pure states for bulk quantum computation. *Phys. Rev. A* **57(5),** May (1998).
23. Ernst, R. R., Bodenhausen, G. & Wokaun, A. *Principles of Nuclear Magnetic Resonance in One and Two Dimensions* (Oxford Univ. Press, Oxford, 1994).
24. Chuang, I. L., Gershenfeld, N., Kubinec, M. G. & Leung, D. W. Bulk quantum computation with nuclear magnetic resonance: Theory and experiment. *Proc. R. Soc. Lond. A* **454,** 447–467 (1998).
25. Warren, W. S. The usefulness of NMR quantum computing. *Science* **277,** 1688–1690 (1997).
26. Jones, T. F. & Mosca, M. Implementation of a quantum algorithm to solve deutsch's problem on a nuclear magnetic resonance quantum computer. *J. Chem. Phys.* (in the press; LANL E-print quant-ph/9801027).

Acknowledgements. We thank A. Pines and M. Kubinec for discussion. This work was supported by DARPA under the NMRQC and QUIC initiatives. L.V. gratefully acknowledges a Francqui Fellowship of the Belgian American Educational Foundation and a Yansouni Family Fellowship.

Correspondence and requests for materials should be addressed to I.L. (e-mail: ichuang@almaden.ibm.com).

Spontaneous formation of ordered structures in thin films of metals supported on an elastomeric polymer

Ned Bowden*, Scott Brittain*, Anthony G. Evans†, John W. Hutchinson† & George M. Whitesides*

** Department of Chemistry and Chemical Biology, Harvard University, 12 Oxford Street, Cambridge, Massachusetts 02138, USA*
† Department of Engineering and Applied Sciences, Harvard University, Pierce Hall, Cambridge, Massachusetts 02138, USA

Spontaneous generation of complex order in apparently simple systems is both arresting and potentially useful[1–11]. Here we describe the appearance of complex, ordered structures induced by the buckling of thin metal films owing to thermal contraction of an underlying substrate. We deposit the films from the vapour phase on a thermally expanded polymer (polydimethylsiloxane, PDMS). Subsequent cooling of the polymer creates compressive stress in the metal film that is relieved by buckling with a uniform wavelength of 20–50 micrometres. The waves can be controlled and orientated by relief structures in the surface of the polymer, which can set up intricate, ordered patterns over large areas. We can account qualitatively for the size and form of the patterned features in terms of the non-uniform stresses developed in the film near steps on the polymer substrate. This patterning process may find applications in optical devices such as diffraction gratings and optical sensors, and as the basis for methods of strain analysis in materials.

Thin metal films—typically 50-nm-thick layers of gold with a 5-nm adhesion interlayer of titanium or chromium—were deposited onto PDMS by electron beam evaporation (Fig. 1). The metal source heats and expands the PDMS substrate before and during deposition. We believe that local heating of the surface of the PDMS also slightly modifies its mechanical properties; perhaps by introducing new crosslinks[12]. After cooling to ambient temperature, the surface appeared frosted, because of light scattering from a network of periodic surface waves (Fig. 2a)[13]. Similar waves were found with a variety of metals, including nickel, aluminum, titanium and chromium. The waves almost disappeared when the sample was reheated to 110 °C, but reformed on cooling. They also formed on PDMS externally heated to 300 °C during the evaporation of metal. Conversely, when the PDMS was cooled to 0 °C during evaporation of metal, waves did not arise; this observation verifies the central importance of the thermal excur-

sion. The waves had periodicities between 20 and 50 μm; their depths, measured from the crest to the trough, ranged from 1.5 μm for evaporations performed without external heating, to 3.9 μm for evaporations conducted at 300 °C. We propose that these waves result from redistribution, by buckling, of compressive stresses that develop in the surface of the sample on cooling from the evaporator temperature to ambient temperature. These waves are similar to those formed in the wrinkling of skin sheets in sandwich structures[14], but different from the waves in buckling-driven film delamination[15] because the metal films remain attached to the PDMS.

On flat, unconstrained PDMS, the waves were disordered, except near an edge. When the PDMS was attached to a glass slide that constrained its expansion on one face, the ordering that occurred reflected, in part, this constraint. To allow the PDMS to contract isotropically, we separated the PDMS, which had been coated with gold and which showed a pattern of waves, from the glass slide with a razor blade. The PDMS was placed on a paper tissue, heated until the waves almost disappeared, and then allowed to cool again. The PDMS expanded and contracted isotropically. The waves reformed with dimensions similar to those observed before, but, in general, in patterns ordered only near relief structures in the PDMS. Strong ordering occurred on evaporating the metal film onto PDMS having a bas-relief pattern on its surface (Fig. 2b–f); these patterns were created by casting PDMS against a 2–20 μm thick patterned photoresist layer[16,17]. The pattern of waves made a transition from

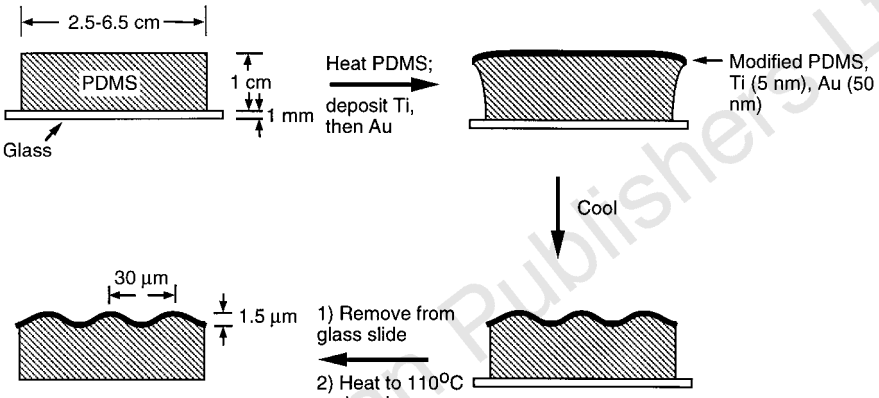

Figure 1 Preparation of metal films on PDMS. A thick (1.0 × 2.5 × 6.5 cm) layer of PDMS was allowed to adhere to a thin glass slide and was loaded into an electron beam evaporator; the chamber was evacuated to a pressure of 10^{-6} torr. The electron beam heated the metal sources; this heat also reached the PDMS and caused it to expand. Here we exaggerate the expansion of the PDMS for clarity; in fact it expands by <1%. The metals were deposited on the expanded PDMS; a typical film comprised 50 Å of titanium evaporated at 1 Å s^{-1}, followed by 500 Å of gold evaporated at 3 Å s^{-1}. After the evaporation, the PDMS cooled and contracted; waves formed on the surface. The PDMS was separated from the glass slide with a razor blade, heated to 110 °C, and cooled to ambient temperature. The pattern of waves before and after separation, heating, and cooling were similar.

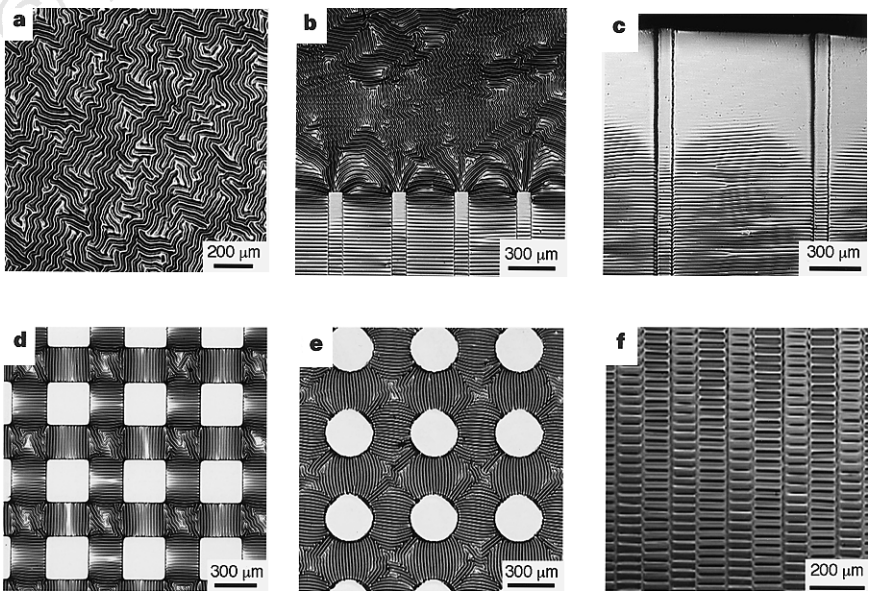

Figure 2 Optical micrographs showing representative patterns of waves that formed when the metals were evaporated onto warm (~110 °C) PDMS, and the sample then cooled to room temperature. **a**, Disordered regions covered flat PDMS far from any steps or edges. **b**, Micrograph showing the transition from disordered waves to waves ordered by rectangular ridges (100 μm wide and 10–20 μm high; separated by 300 μm). **c**, A flat, waveless region of gold near an edge in the PDMS gradually became a system of waves ordered by the rectangular ridges (100 μm wide and 10–20 μm high; separated by 800 μm). **d**, **e**, Flat squares (300 μm on each side) and circles (150 μm in radius) elevated by 10–20 μm relative to the surface showed no buckling on the plateaux, but ordered patterns of waves on the recessed regions between them. **f**, Rectangular ridges (100 μm wide and 10–20 μm high; separated by 100 μm) aligned the waves parallel to the direction of the raised portions of the PDMS. These pictures are representative of the patterns that form over the whole surface area for each sample (up to 25 cm^2). The PDMS was coated with 5 nm of titanium or chromium and 50 nm of gold.

disordered (Fig. 2a) to ordered (Fig. 2b–f) when located within 200–600 μm of a step or edge.

We have developed a model that relates the spatially non-uniform stresses in a metal film on patterned PDMS to the wave patterns. This model correctly estimates the circumstances in which waves initiate, as well as their orientation and wavelength. We describe this model for two systems: (1) a single thin, stiff surface film on a thick, homogeneous compliant substrate, representing Au on PDMS, and (2) a multilayer film, representing Au on PDMS having a surface layer with modified properties (Fig. 3).

If the PDMS were perfectly smooth and the film unbuckled, then at temperatures T below the deposition temperature T_D, the film would be in a state of uniform, equi-biaxial compressive stress σ_o(Pa) given by equation (1) (ref. 18):

$$\sigma_o = \frac{E_m(\alpha_p - \alpha_m)(T_D - T)}{(1 - \nu_m)} \quad (1)$$

Here the subscripts m and p refer to the metal film and PDMS, respectively, ν (unitless) is the Poisson's ratio, α ($°C^{-1}$) is the coefficient of thermal expansion, and E (Pa) is the Young's modulus. The parameters for gold and PDMS are: $E_m = 82$ GPa, $E_p = 20$ MPa, $\nu_m = 0.33$ and $\nu_p = 0.48$. The equi-biaxial compressive film stress arises from the considerable mismatch of the coefficients of thermal expansion of the PDMS and the film ($\alpha_p \approx 20\alpha_m$).

As the temperature drops and the compressive stresses in the film increase, buckling starts where the maximum principal compressive stress attains the critical value, σ_{crit} (Pa; equation (2))[14]. The associated sinusoidal wave pattern, aligned perpendicular to the direction of maximum compression, has wavelength L (m) given by equation (3)[14]. Here t (m) is the film thickness.

$$\sigma_{crit} \approx 0.52 \left(\frac{E_m}{(1 - \nu_m^2)}\right)^{1/3} \left(\frac{E_p}{(1 - \nu_p^2)}\right)^{2/3} \quad (2)$$

$$L \approx 4.36t \left(\frac{E_m(1 - \nu_p^2)}{E_p(1 - \nu_m^2)}\right)^{1/3} \approx 4.4t \left(\frac{E_m}{E_p}\right)^{1/3} \approx 61t \quad (3)$$

Because the film is stiff relative to the PDMS, the wavelength is many times the film thickness. Equation (3) yields an estimate: $L \sim 3.4$ μm. As the observed value of L is approximately nine times larger than this estimate, we conclude that this model is oversimplified. In practice, we believe that the heating occurring during the metal deposition also modifies the top surface of the PDMS (plausibly by thermal crosslinking), generates compressive stress, and alters its Young's modulus, perhaps to a depth of the order of 1 μm. This modification creates a multilayered film with an effective bending stiffness larger than that of the thin metal film, and increases the wavelength (Fig. 3). A modified PDMS layer of thickness 2 μm (40 times that of the Au) with a plausible Young's modulus ($E_1 \approx 80$ MPa $\approx 4E_p$) increases the wavelength by a factor of 7, in satisfactory agreement with the experimental result. Uncertainty with respect to the properties and structure of the modified PDMS layer makes it difficult to provide a more quantitative comparison.

In an equi-biaxial state of stress, there is neither a preferred orientation for the waves, nor a reason for the waves to form systematic patterns. When steps are present, however, the stress in

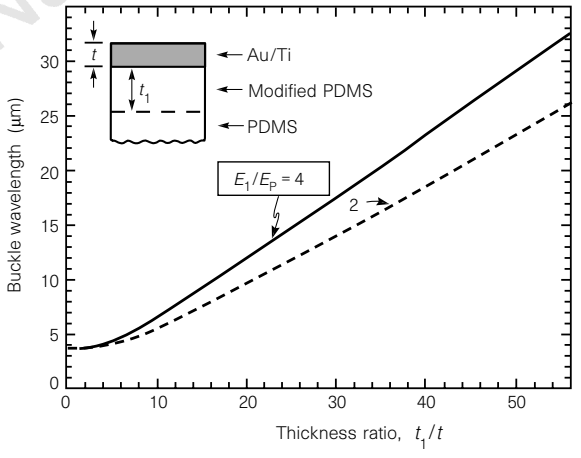

Figure 3 How the wavelength changes with a modified layer of PDMS at the surface. We assume that a uniform, modified layer of PDMS of thickness t_1 and Young's modulus E_1 exists between the gold of thickness t and PDMS. The wavelength increases as the thickness of the modified layer of PDMS is increased relative to the thickness of the gold film, and as the ratio E_1/E_p is increased.

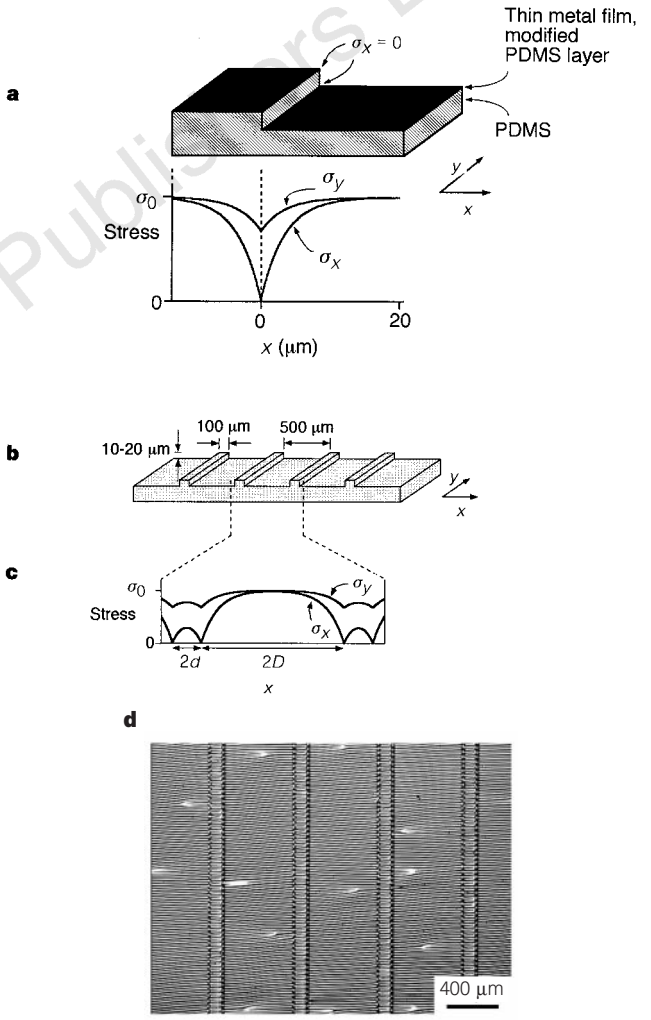

Figure 4 Ordering of waves on a surface of PDMS patterned in a bas-relief structure. **a**, We assume that in-plane displacement normal to the line of a step in the PDMS (2–20 μm high) relieves the compressive stress in the metal film; that is, $\sigma_x = 0$ at the step. The graph shows σ_x and σ_y as a function of x at a step in the PDMS (from equations (4a) and (4b)). The variation in σ_y as a function of x is due to a Poisson effect where the stress in the y-direction is partially relieved by expansion of the metal film into the x-direction. **b**, The surface of the PDMS was patterned into regions 100-μm wide that were raised by 10-20 μm and separated by 500 μm; 5 nm of titanium and 50 nm of gold were deposited on this surface. **c**, The stress in the system followed equations (6a) and (6b). The pattern of waves in Fig. 2c follows the distribution of stress predicted by equations (6a) and (6b). **d**, An optical micrograph picture of the PDMS surface after buckling. The waves are aligned perpendicular to the steps and in the direction of the greater stress.

the film will no longer be uniform or equi-biaxial. There is a strong orientation to the stress in the vicinity of the steps, with an associated maximum principal compressive stress direction at each point. The wave pattern develops with crests aligned perpendicular to the direction of maximum compressive stress.

The non-uniform pre-buckling stress around steps is derived from a model that approximates the influence of the substrate on the thin film as an attached elastic foundation of springs exerting only tangential forces. The PDMS offers little resistance to displacement of the film in the direction perpendicular to the step; this displacement relieves the stress in that direction, becoming zero at the step itself. A solution for the stresses on either side of an infinitely long isolated step coincident with the y-axis (Fig. 4a) gives equations (4a) and (4b), where σ_x is the stress in the x-direction, σ_y is the stress in the y-direction, and x is measured starting from the step. The transition length l (m) characterizing the distribution of stress from the step to the remote smooth film is given by equation (5).

$$\sigma_x = -\sigma_0[1 - e^{-|x|/l}] \tag{4a}$$

$$\sigma_y = -\sigma_0[1 - \nu_m e^{-|x|/l}] \tag{4b}$$

$$l \approx 0.3t\left[\frac{E_m(1-\nu_p^2)}{E_p(1-\nu_m^2)}\right] \approx 0.3t\left[\frac{E_m}{E_p}\right] \approx 1{,}060t \tag{5}$$

The transition length is 17 times the buckle wavelength, L, for the gold/PDMS system.

The predictability of the wave patterns is demonstrated by analysis of an array of long straight strips parallel to the y-axis, width $2d$, separated by $2D$ (Fig. 4b). The stress distribution in the film before buckling is given by equations (6a) and (6b), for ($|x| < d$) where x is measured from the centre of the strip (Fig. 4c).

$$\sigma_x = -\sigma_0\left[1 - \frac{\cosh(x/l)}{\cosh(d/l)}\right] \tag{6a}$$

$$\sigma_y = -\sigma_0\left[1 - \nu_m\frac{\cosh(x/l)}{\cosh(d/l)}\right] \tag{6b}$$

The stresses between the strips are given by the same formulae, but with d replaced by D, and with x now measured from the centre of that region. We note that the compressive stress in the y-direction remains relatively large, with a minimum, $-\sigma_0(1-\nu_m)$ at the step; the compressive stress in the x-direction is smaller everywhere, and zero at the step. Consistent with σ_y being larger than σ_x, the wave pattern shows crests aligned perpendicular to the y-axis (Fig. 4d).

The process described here provides a remarkable example of the spontaneous generation of complexity. The regularity in the waves reflects the uniformity in the physical properties and dimensions of the materials. The ability to control the orientation and periodicity of these waves by changing these parameters, and by patterning the surface of the PDMS using straightforward techniques, makes this system eminently controllable. We believe that this process offers potential to generate planar and non-planar surfaces patterned in 1–100 μm features over many square centimetres. Such patterns are interesting for their potential applications in sensors and optical components (for example, diffraction gratings): they also allow mapping of material properties in two dimensions. Most interestingly, such patterns offer the opportunity to study the generation of complex ordered structure from simple patterns. □

Received 7 January; accepted 16 March 1998.

1. Whitesides, G. M., Mathias, J. P. & Seto, C. T. Molecular self-assembly and nanochemistry: a chemical strategy for the synthesis of nanostructures. *Science* **254,** 1312–1319 (1991).
2. Desiraju, G. R. *Crystal Engineering: The Design of Organic Solids* (Elsevier, New York, 1989).
3. van Blaaderen, A., Ruel, R. & Wiltzius, P. Template-directed colloidal crystallization. *Nature* **385,** 321–324 (1997).
4. Bain, C. D. *et al.* Formation of monolayer films by the spontaneous assembly of organic thiols from solution onto gold. *J. Am. Chem. Soc.* **111,** 321–335 (1989).
5. Voet, D. & Voet, J. G. *Biochemistry* (Wiley, New York, 1995).
6. Davis, M. E., Lobo, R. F. Zeolite and molecular sieve synthesis. *Chem. Mater.* **4,** 756–768 (1992).
7. Lewis, D. W., Willock, D. J., Catlow, C. R. A., Thomas, J. M. & Hutchings, G. J. De novo design of structure-directing agents for the synthesis of microporous solids. *Nature* **382,** 604–606 (1996).
8. Makse, H. A., Havlin, S., King, P. R. & Stanley, H. E. Spontaneous stratification in granular mixtures. *Nature* **386,** 379–382 (1997).
9. Jaeger, H. M. & Nagel, S. R. Physics of the granular state. *Science* **255,** 1523–1531 (1992).
10. Zik, O., Levine, D., Shtrikman, S. G. & Stavans, J. Rotationally induced segregation of granular materials. *Phys. Rev. Lett.* **73,** 644–647 (1994).
11. Knight, J. B., Jaeger, H. M. & Nagel, S. R. Vibration-induced size separation in granular media: the convection connection. *Phys. Rev. Lett.* **70,** 3728–3731 (1993).
12. Bodo, P. & Sundgren, J.-E. Titanium deposition onto ion-bombarded and plasma-treated polydimethylsiloxane: surface modification, interface, and adhesion. *Thin Solid Films* **136,** 147–159 (1986).
13. Martin, G. C. *et al.* The metallization of silicone polymers in the rubbery and the glassy state. *J. Appl. Phys.* **53,** 797–799 (1982).
14. Allen, H. G. *Analysis and Design of Structural Sandwich Panels* (Pergamon, New York, 1969).
15. Hutchinson, J. W., Thouless, M. D. & Liniger, E. G. Growth and configuration stability of circular, buckling-driven film delaminations. *Acta Metall. Mater.* **40,** 295–308 (1992).
16. Kumar, A., Abbott, N. L., Kim, E., Biebuyck, H. A. & Whitesides, G. M. Patterned self-assembled monolayers and meso-scale phenomena. *Acc. Chem. Res.* **28,** 219–226 (1995).
17. Xia, Y. & Whitesides, G. M. Soft Lithography. *Angew. Chem. Int. Edn* **37,** 550–575 (1998).
18. Ohring, M. *The Material Science of Thin Films* (Academic, San Diego, 1992).

Acknowledgements. We thank D. Munn for helpful discussions. This work was supported by the NSF, the Office of Naval Research, and the Defense Advanced Research Projects Agency. N.B. thanks the Department of Defense for a predoctoral fellowship.

Correspondence and requests for materials should be addressed to G.M.W. (e-mail: gwhitesides@gmwgroup.harvard.edu).

Polymer gels with engineered environmentally responsive surface patterns

Zhibing Hu*, Yuanye Chen*, Changjie Wang*, Yindong Zheng* & Yong Li†

* *Department of Physics, University of North Texas, Denton, Texas 76203, USA*
† *Kimberly-Clark Corporation, Neenah, Wisconsin 54956, USA*

The polymer gels called hydrogels may be induced to swell or shrink (taking up or expelling water between the crosslinked polymer chains) in response to a variety of environmental stimuli, such as changes in pH or temperature, or the presence of a specific chemical substrate[1]. These gels are being explored for several technological applications, particularly as biomedical materials[2]. When hydrogels swell or shrink, complex patterns may be generated on their surfaces[3–7]. Here we report the synthesis and controlled modulation of engineered surface patterns on environmentally responsive hydrogels. We modify the character of a gel surface by selectively depositing another material using a mask. For example, we use sputter deposition to imprint the surface of an *N*-isopropylacrylamide (NIPA) gel with a square array of gold thin films. The periodicity of the array can be continuously varied as a function of temperature or electric field (which alter the gel's volume), and so such an array might serve as an optical grating for sensor applications. We also deposit small areas of an NIPA gel on the surface of an acrylamide gel; the patterned area can be rendered invisible reversibly by switching the temperature above or below the lower critical solution temperature of the NIPA gel. We anticipate that these surface patterning techniques may find applications in display and sensor technology.

We first discuss the surface patterns made by use of the sputtering-deposition technique. *N*-isopropylacrylamide (NIPA) gel slabs were made by free-radical polymerization, as follows. A mixture of 7.8 g of *N*-isopropylacrylamide, 133 mg of methylene-bis-acrylamide as a crosslinker, and tetramethylethylenediamine (240 μl) as an accelerator, was dissolved in 100 ml of deionized and distilled water. Nitrogen gas was bubbled through the solution to remove dissolved oxygen. The polymerization was initiated by adding 40 mg of ammonium persulphate. The samples were kept in water for several days to wash out chemical residues. The NIPA gels were then